Research article

NMR IN BIOMEDICINE

Received: 11 March 2015, Revised: 6 August 2015, Accepted: 7 August 2015, Published online in Wiley Online Library: 16 September 2015

(wileyonlinelibrary.com) DOI: 10.1002/nbm.3388

Cerebral multifrequency MR elastography by remote excitation of intracranial shear waves

Andreas Fehlner[a], Sebastian Papazoglou[a], Matthew D. McGarry[b], Keith D. Paulsen[b], Jing Guo[a], Kaspar-Josche Streitberger[a], Sebastian Hirsch[a], Jürgen Braun[c] and Ingolf Sack[a]*

The aim of this study was to introduce remote wave excitation for high-resolution cerebral multifrequency MR elastography (mMRE). mMRE of 25–45-Hz drive frequencies by head rocker stimulation was compared with mMRE by remote wave excitation based on a thorax mat in 12 healthy volunteers. Maps of the magnitude $|G^*|$ and phase φ of the complex shear modulus were reconstructed using multifrequency dual elasto-visco (MDEV) inversion. After the scan, the subjects and three operators assessed the comfort and convenience of cerebral mMRE using two methods of stimulating the brain. Images were acquired in a coronal view in order to identify anatomical regions along the spinothalamic pathway. In mMRE by remote actuation, all subjects and operators appreciated an increased comfort and simplified procedural set-up. The resulting strain amplitudes in the brain were sufficiently large to analyze using MDEV inversion, and yielded high-resolution viscoelasticity maps which revealed specific anatomical details of brain mechanical properties: $|G^*|$ was lowest in the pons (0.97 ± 0.08 kPa) and decreased within the corticospinal tract in the caudal–cranial direction from the crus cerebri (1.64 ± 0.26 kPa) to the capsula interna (1.29 ± 0.14 kPa). By avoiding onerous mechanical stimulation of the head, remote excitation of intracranial shear waves can be used to measure viscoelastic parameters of the brain with high spatial resolution. Therewith, the new mMRE method is suitable for neuroradiological examinations in the clinic. Copyright © 2015 John Wiley & Sons, Ltd.

Keywords: MR elastography; *in vivo* multifrequency MRE; brain; intracranial shear strain; viscoelasticity; high resolution; corticospinal tract; pons

INTRODUCTION

Many diseases are associated with a change in the viscoelastic properties of soft tissues, as evidenced by the well-known sensitivity of manual palpation. Cerebral MR elastography (MRE) is a new imaging modality which brings viscoelastic property measurements into the workscope of neuroradiologists (1–3). Previous pilot studies have demonstrated the sensitivity of cerebral MRE to a variety of neurological disorders, such as multiple sclerosis (4,5), Alzheimer's disease (6), Parkinson's disease (7), amyotrophic lateral sclerosis (8), normal pressure hydrocephalus (9,10) and tumors (11,12). The use of cerebral MRE for diagnostic purposes has been supported by several studies in mouse brain, which have demonstrated sensitivity to demyelination, inflammation and extracellular matrix degeneration (13–16). Current efforts in brain MRE have been invested in revealing the topology of viscoelastic properties of brain tissue *in vivo* (17–19).

Cerebral MRE relies on the excitation and measurement of shear waves inside the brain. Other than a single pilot study which exploited intrinsic pulsation (20), intracranial shear waves in MRE have been produced by bite bar drivers (1,2,21), pneumatic cushions (22–24), head rockers placed underneath the dorsal cranium (3,25) or table resonances (26). The measured wave fields are analyzed for the underlying viscoelastic material properties by mathematical algorithms capable of solving the time-harmonic elastic inverse problem (27,28). Our method of choice is a direct inversion of the Helmholtz equation, which combines multiple wave fields at different excitation frequencies to increase the robustness of the inverse problem solution (29). This multifrequency approach improves the quality of viscoelastic parameter maps by including more experimental data. For instance, in a recent multifrequency MRE (mMRE) study of brain tissue, four drive frequencies (30, 40, 50 and 60 Hz) were used to produce viscoelastic parameter maps of the magnitude $|G^*|$ and phase angle φ of the complex shear modulus. Property image resolution was sufficient to distinguish brain anatomy, such as the corpus callosum, caudate nucleus and the thalamus (18).

* *Correspondence to: I. Sack, Department of Radiology, Charité – Universitätsmedizin Berlin, Charitéplatz 1, 10117 Berlin, Germany. E-mail: ingolf.sack@charite.de*

a *A. Fehlner, S. Papazoglou, J. Guo, K.-J. Streitberger, S. Hirsch, I. Sack*
Department of Radiology, Charité – Universitätsmedizin Berlin, Berlin, Germany

b *M. D. McGarry, K. D. Paulsen*
Thayer School of Engineering, Dartmouth College, Hanover, NH, USA

c *J. Braun*
Institute of Medical Informatics, Charité – Universitätsmedizin Berlin, Berlin, Germany

Abbreviations used: *CC, crus cerebri; CI, capsula interna; CST, corticospinal tract; MDEV inversion, multifrequency dual elasto-visco inversion; MEG, motion-encoding gradient; mMRE, multifrequency MR elastography; OSS, octahedral shear strain; SD, standard deviation.*

NMR IN BIOMEDICINE

In order to enhance cerebral MRE for the clinic, the method should be optimized with respect to the range and number of mechanical frequencies and the driver set-up to ensure a comfortable examination, ideally without compromising the resolution of the viscoelasticity maps. Direct actuation of the head can be uncomfortable – an indirect transfer of wave energy into the cranial cavity would avoid direct head actuation and potentially increase the patient population able to undergo cerebral MRE.

This study develops a more comfortable MRE examination of the head over a broad frequency range in order to facilitate viscoelasticity imaging of brain tissue with high spatial resolution.

To this end, we applied remote actuation brain mMRE to a group of 12 healthy volunteers, each of whom was scanned with coronal slice orientation in order to explore different areas of the brain along the spinothalamic pathway, such as the pons, crus cerebri (CC) and capsula interna (CI). For validation, the viscoelastic properties were compared with results obtained in the same group examined by a head cradle. Therewith, we pursue cerebral mMRE without onerous head stimulation for improved patient comfort, so that the technique can be applied to a wide range of neuroradiological conditions.

METHODS

Subjects

The study was approved by our institutional review board and written informed consent was obtained from all participants prior to the examination. The brains of 12 healthy volunteers (nine men; mean age, 34.0 ± 10.2 years; range, 27–54 years; body mass index, 23.1 ± 2.7) were scanned twice by mMRE, once with head-cradle-based mechanical stimulation (18) and a second time using the new actuation principle described in detail below.

Remote excitation of cerebral vibrations

The new driver set-up for brain MRE is shown in Fig. 1. A mat of compressed hard rubber of 39 × 20 cm^2, with a thickness of 1.5 cm and density of 0.77 g/cm^3, was placed on the volunteer's thorax and fixed by Velcro stripes. The mat was mounted on a remote nonmagnetic vibration generator at the distal end of the MRI table, which generated motion of ±2 mm deflection amplitude primarily along the subject's cranial–caudal axis (18). Five vibration frequencies were applied from 25 to 45 Hz in increments of 5 Hz.

Wave image acquisition

All experiments were performed on a 1.5-T MRI scanner (Magnetom Sonata; Siemens, Erlangen, Germany) using a four-channel head coil. A single-shot spin-echo echo-planar imaging sequence, with trapezoidal flow-compensated motion-encoding gradients (MEGs) consecutively applied along all three axes of the scanner coordinate system, was used for rapid motion field acquisition (30). To allow the mechanical waves to travel into the cranial cavity, the vibration was initiated through a trigger pulse by the scanner at least 100 ms before the start of the MEG. In eight repetitive scans, this delay was decreased by increments of one-eighth of a vibration period to capture the dynamics of a full wave cycle. Nine contiguous wave image slices of 2 × 2 × 2-mm^3 resolution, five frequencies, eight wave dynamics and three MEG directions (yielding a total of 1080 images) were acquired in a coronal view through the regions of the pons, CC and CI. This view covers the wave propagation pathway along the cranial–caudal axis, which is of special interest for the analysis of the attenuation properties of remotely induced shear waves. Other imaging parameters were as follows: TR = 2170 ms; TE = 99 ms; field of view, 192 × 176 mm^2; matrix size, 88 × 96; MEG frequencies (number of MEG cycles) of 25 Hz (1), 25 Hz (1), 25 Hz (1), 30 Hz (1) and 50 Hz (2), corresponding to vibration frequencies of 25, 30, 35, 40 and 45 Hz, respectively [note that the MEG frequency and cycle number were chosen to accomplish the highest encoding efficiency within the given TE according to the principle of fractional motion encoding (31)]; MEG amplitude, 30 mT/m; scan time for each frequency of ~1 min, resulting in a total acquisition time of ~5 min for a full mMRE examination.

Multifrequency dual elasto-visco (MDEV) inversion-based high-resolution MRE

We applied MDEV inversion to generate high-resolution maps of viscoelastic properties, as described in greater detail in ref. (32).

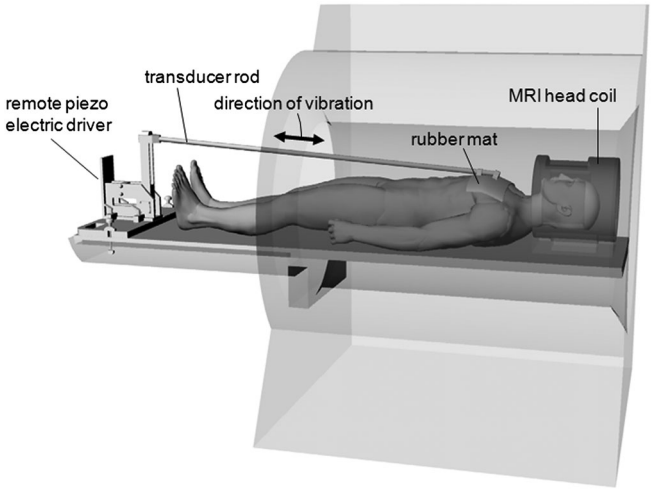

Figure 1. Remote driver set-up based on a thorax mat connected to a nonmagnetic driver at the end of the patient table. The rubber mat is coupled to the patient thorax by a Velcro belt.

Briefly, MDEV inversion was applied to the low-pass-filtered in-plane derivative components $[u^*_{j,k}(\omega_l)$ with $k = 1, 2]$ obtained by gradient-based unwrapping, which reflect mainly shear deformation assuming that the spatial gradients sufficiently suppressed long-wavelength longitudinal waves and rigid body motion. MDEV inversion by equations (2a) and (2b) in ref. (32) provides maps of $|G^*|$ and φ according to two independent solutions of the Helmholtz equation for the magnitude and phase of the complex shear modulus G^*. The overall shear strain was quantified by the volumetric average of the octahedral shear strain (OSS) (33), which provides a scalar measure of the shear strain suitable for testing the performance of drivers in shear wave-based elastography.

Assessment of the volunteer's comfort and operator convenience

Immediately after the examination with either the head cradle or remote driver, each subject was asked in a questionnaire to grade three sources of discomfort imposed by the mMRE vibration set-up (see Table 1): (1) the subjectively felt strength of the vibration; (2) the discomfort related to constrictions and positioning of the body and the head; and (3) the perceived level of acoustic noise produced by the actuator relative to the scanner noise. Furthermore, three experienced brain MRE operators were asked to grade their effort in setting up the MRE drivers. Points included in the questionnaire were as follows: (1) the time for the education and instruction of patients (anticipated from the instructions given to the volunteers); (2) the time and effort for head or body positioning inside the cradle, radiofrequency coil and scanner; and (3) the effort necessary to complete the entire actuator set-up.

Statistical analysis

Statistical analysis was performed using GraphPad Prism v.5 (GraphPad software, La Jolla, CA, USA) with a level of significance of 0.05. For the analysis of $|G^*|$ and φ values in different brain regions, specific tissue structures were manually segmented on the basis of the MRE magnitude images: pons, CC and CI (see Fig. 4, 'Results' section). OSS and wave amplitudes were analyzed in two regions: the whole brain parenchyma (excluding the ventricles) and a combined region of the pons, CC and CI. Similar to the pons, CC and CI, whole brain parenchyma was manually segmented on the basis of MRE magnitude images (in the following, referred to as full brain region). Results were tabulated as the arithmetic mean ± standard deviation (SD). Regional differences were analyzed by Friedmann's test followed by Dunn's multiple comparison. Differences in wave amplitudes, OSS values and assessment scores between mMRE methods were analyzed by Wilcoxon signed-rank test. Normal distribution was not assumed because of the limited number of subjects. The symmetric data distribution around the medians of the wave amplitudes and OSS was confirmed by sign tests.

RESULTS

The new remote brain actuator was well tolerated by all subjects and better received than the head cradle, as indicated by the overall scores given in Table 1 (2.1 ± 0.4 *versus* 2.7 ± 0.3, $p = 0.02$). Notably, the chest mat was equally well assessed by women and men, indicating a minor influence of thorax volume on the efficiency of wave excitation. Moreover, no limitations caused by breathing were encountered.

Most obvious, the acoustic burden imposed by the driver was strongly reduced ($p = 0.047$) as no vibration was produced near the ears. In addition, the vibration of the head cradle was rated as uncomfortable (grade 4 out of 5, see Table 1) by three of the 12 volunteers; only one subject felt a medium level of discomfort (grade 3) from the thorax mat ($p = 0.043$). In contrast, the positioning of the drivers was not rated differently by subjects ($p = 0.556$), whereas operators were particularly positive about the fact that the remote set-up was entirely detached from the head which helped to mitigate concerns about cerebral vibrations.

Figure 2 illustrates the real-part shear wave images from the three curl components of the wave field in a coronal view and at each of the five vibration frequencies used in this study. These results clearly illustrate that the wavelength of the induced mechanical waves decreases with increasing excitation frequency.

Cerebral wave amplitudes averaged within the full brain region and produced by the remote actuator were similar to those encountered in mMRE with the head cradle (see Fig. 3a). The amplitude generated by the remote actuator and averaged over all vibration frequencies was 9.66 ± 3.83 μm, which is similar to the value of 10.18 ± 5.67 μm produced by the head cradle ($p = 0.69$). In addition, OSS (see Fig. 3b) was not significantly altered by our remote vibration set-up compared with the head cradle [(0.56 ±

Table 1. Subjective assessment of comfort and operator convenience of mechanical drivers in cerebral multifrequency MR elastography (mMRE) by 12 healthy volunteers and three operators. Values in parentheses denote the standard deviation (SD) and the range of the values

	Remote actuation	Head cradle
Assessment of discomfort by the volunteer (1, negligible; 5, very uncomfortable)		
Vibration	2.1 (0.7; 2–4)	2.9 (0.8; 2–4)
Positioning (constriction, cushions, head pad)	2.4 (1.0; 1–4)	2.8 (0.8; 2–4)
Acoustic noise (relative to the scanner's gradient system)	1.7 (0.9; 1–3)	2.4 (0.7; 1–3)
Mean score	2.1 (0.4)	2.7 (0.3)
Assessment of effort by three operators (1, no additional effort; 5, hard to implement)		
Patient instruction	1, 2, 1	3, 3, 3
Patient positioning	2, 2, 2	3, 3, 2
Actuator set-up	2, 2, 2	2, 2, 2

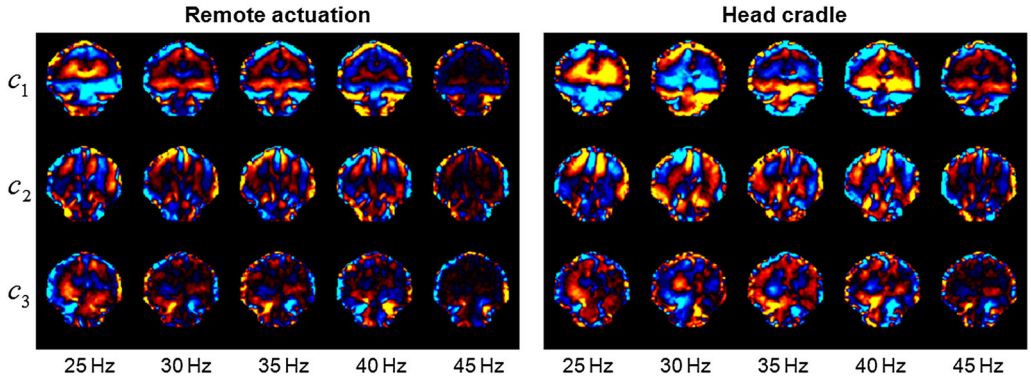

Figure 2. Real-part shear wave images from the three curl components of the wave field in coronal view at five drive frequencies, illustrating the shear strain induced by the remote driver and the head cradle. The strain images are scaled from -1×10^{-3} to 1×10^{-3}.

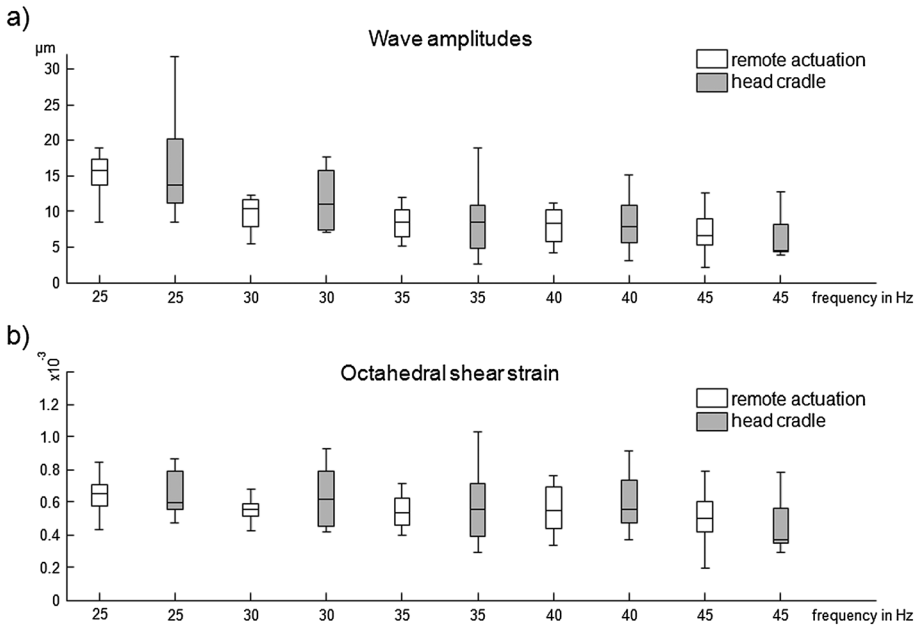

Figure 3. Group mean values of the wave amplitudes (a) and octahedral shear strain (OSS) (b) for different frequencies and actuation methods averaged within the full brain region.

$0.12) \times 10^{-3}$ *versus* $(0.59 \pm 0.21) \times 10^{-3}$, $p = 0.37$]. Accounting for the specific regions CI, CC and pons, we observed no differences in either amplitudes or OSS within these regions [amplitude with remote actuator, 10.92 ± 4.50 µm; amplitude with head cradle, 11.84 ± 6.84 µm; $p = 0.45$; OSS with remote actuator, $(0.58 \pm 0.15) \times 10^{-3}$; OSS with head cradle, $(0.64 \pm 0.26) \times 10^{-3}$; $p = 0.16$]. As shown in Fig. 3, SDs and data ranges corresponding to the remote actuator appear to be lower than those produced by the head cradle, which is, however, statistically insignificant and considered as a trend (mean amplitude SD of remote actuator, 2.59 µm; mean amplitude SD of head cradle, 4.49 µm; $p = 0.06$; mean OSS SD of remote actuator, 0.12×10^{-3}; mean OSS SD of head cradle, 0.20×10^{-3}; $p = 0.06$).

MDEV inversion inherently averages over frequency, but allows for spatially resolved parameter maps as shown in Fig. 4. Both actuation settings present similar viscoelastic maps. Group mean values of the regions demarcated in the MRE magnitude images of Fig. 4 are shown in Fig. 5. No significant differences in viscoelastic parameters were observed between the two drivers.

Within the corticospinal tract (CST), $|G^*|$ decreased in the caudal–cranial direction from CC (remote actuator, 1643 ± 265 Pa; head cradle, 1577 ± 316 Pa; $p = 0.73$) to CI (remote actuator, 1294 ± 137 Pa; head cradle, 1273 ± 161 Pa; $p = 0.57$) ($|G^*|$ CC *versus* CI: $p < 0.01$ for both drivers). The pons displayed the lowest $|G^*|$ values of 971 ± 82 Pa by remote actuation and 920 ± 66 Pa by head cradle vibrations (CI *versus* pons: $p < 0.001$ for both drivers). However, Dunn's multiple comparison revealed significant differences between CI and CC only in the remote driver data, further highlighting the lower variability of the data by this set-up (Fig. 5).

Interestingly, the fibers in the lower part of the CST showed greater dissipative behavior (large φ values) than in the other regions, as reflected by the low intensity of CI in the φ maps (Fig. 4). We attribute the low φ values inside the ventricles to noise rather than to the intrinsic mechanical properties of the free fluid. The significance of regional differences in the viscoelastic properties of brain tissue is indicated in Fig. 5. Table 2 summarizes all values of $|G^*|$ and φ.

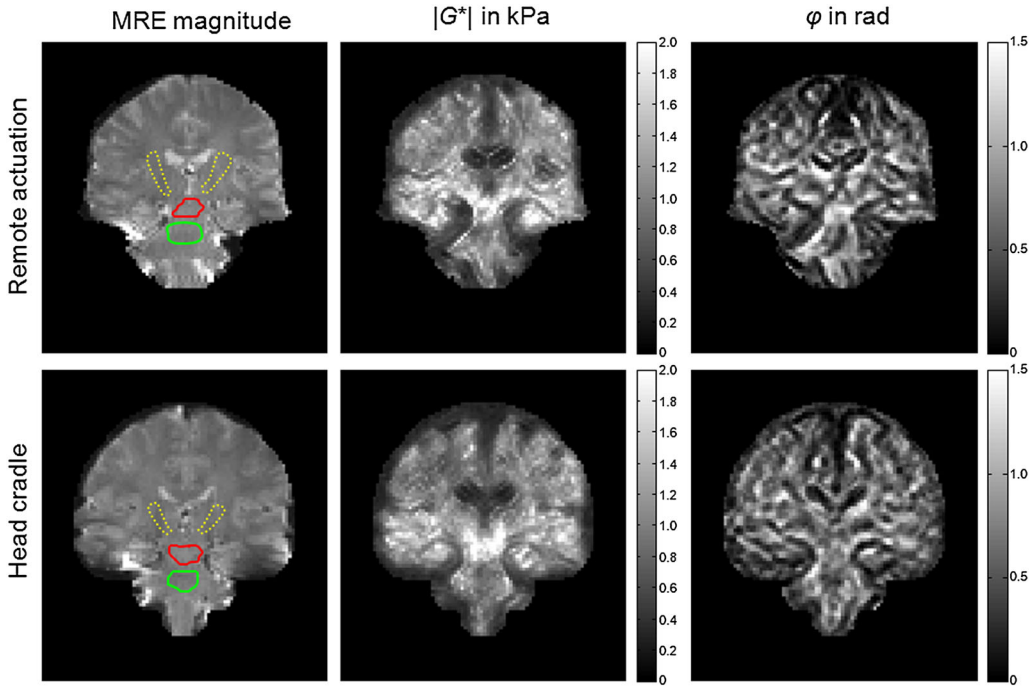

Figure 4. Example parameter maps of $|G^*|$ and φ in coronal views through the brain generated by the two actuation methods (remote, top row; head cradle, bottom row). Regions of interest are demarcated in the MR elastography (MRE) magnitude images and correspond to the corticospinal tract (CST) (capsula interna, CI; dotted yellow line), CST (crus cerebri, CC; red line) and pons (green line).

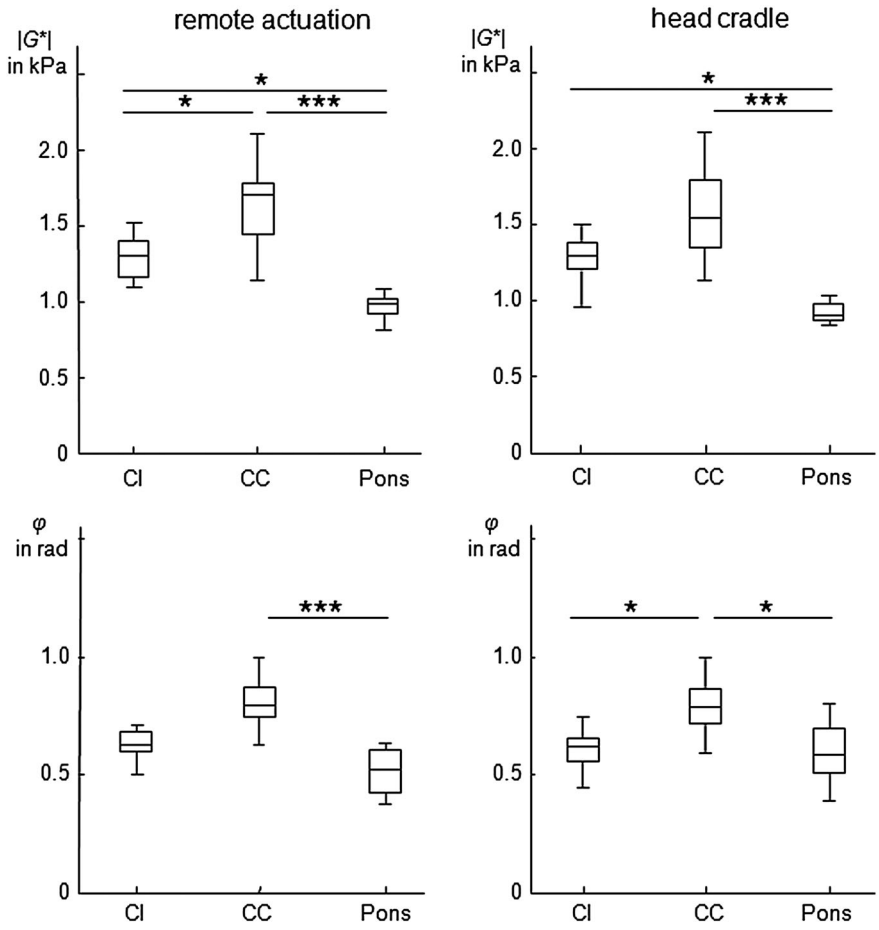

Figure 5. Group mean values of the MR elastography (MRE) parameters $|G^*|$ and φ for capsula interna (CI), crus cerebri (CC) and pons for both actuation methods. Asterisks indicate levels of significance estimated by multiple comparison, corresponding to $^*p < 0.05$ and $^{***}p < 0.001$.

NMR IN BIOMEDICINE

Table 2. Viscoelastic parameters in three brain regions based on multifrequency dual elasto-visco (MDEV) inversion (standard deviations are given in parentheses)

	Remote actuation		Head cradle	
	$\|G^*\|$ (Pa)	φ (rad)	$\|G^*\|$ (Pa)	φ (rad)
Capsula interna	1294 (137)	0.628 (0.062)	1273 (161)	0.603 (0.090)
Crus cerebri	1643 (265)	0.825 (0.153)	1577 (315)	0.792 (0.114)
Pons	971 (82)	0.512 (0.095)	920 (65)	0.590 (0.124)

Discussion

MRE of the brain is an active area of research. The intracranial shear modulus provides a novel source of diagnostic information sensitive to the tissue's micro-architecture which can be exploited clinically, similarly to the success of elastography in the detection of hepatic fibrosis (34,35). This study introduces a method of brain mechanical stimulation which is applicable to patients concerned about the discomfort associated with cerebral mMRE.

Despite the similar wave amplitudes inside the cranial cavity produced by both actuation methods, the manner in which the waves travel whilst becoming attenuated apparently matters. Although the head cradle induces peak amplitudes near the skull, the remote actuator concept relies on pre-attenuated amplitudes before the waves enter the head region. This new concept apparently reduces the mechanical burden of MRE of the brain.

The reduced mechanical burden, combined with fast imaging, enabled us to acquire a rich set of data in brain MRE (full wave fields, five frequencies), which were used to produce high-resolution mechanical images and analysis of $|G^*|$ and φ parameters in CC, CI and pons for the first time.

We demonstrated that remote actuation of intracranial vibrations in a low-frequency range is feasible with shear wave and shear strain amplitudes similar to those of conventional direct head stimulation. Moreover, the remotely induced vibration amplitudes varied to a lesser extent than those produced by the head cradle, suggesting that the influences of head positioning on the efficiency of shear wave transfer into the brain are reduced when shear waves propagate through the chest and spine into the brain.

We analyzed vibration frequencies below the range usually applied in MRE (19,36–38), and obtained maps of the mechanical structure of the brain at a resolution similar to that of previous work (18,32,39). Low vibration frequencies are less damped in soft biological tissue; therefore, they require smaller surface amplitudes relative to high-frequency waves. Combined with a remote wave generator placed on the thorax, low-frequency brain MRE was no more onerous than any conventional neuro-MRI examination.

The values measured by our new set-up are similar to those published previously (18) for white matter delineated in axial slices ($|G^*| = 1252 \pm 260$ Pa), which, in turn, are comparable with values for our current white matter region of CI ($|G^*| = 1294 \pm 137$ Pa).

Comparison of $|G^*|$ and φ values with the storage and loss moduli reported by other groups (17,19,40,41) is not particularly instructive because of the inherent frequency averaging implied by MDEV inversion, and the lower frequency range applied relative to that more commonly exploited in cerebral MRE. Averaging of the dispersion properties of the shear modulus naturally relates all parameters obtained to the center frequency within the applied frequency band. However, this applies to all time-harmonic elastography studies which do not incorporate the fitting of an appropriate viscoelastic model. Another barrier to direct comparison with other literature values is the difference in spatial resolution, as our $|G^*|$ and φ maps estimate the mechanical footprint of tissue heterogeneities, including cerebrospinal fluid-filled sulci, blood vessels and crossing fibers, which are normally smoothed by single-frequency direct inversion strategies (29).

Higher resolution MDEV inversion of our MRE data is potentially useful for the noninvasive characterization of intracranial tumors (11,12,32,42) or for the measurement of localized degenerative effects in the viscoelastic matrix of brain tissue, as observed preliminarily in previous studies (7). To this end, a consistent spatially resolved reference database of the mechanical properties of the human brain is required, including the regions explored in this study.

Moreover, with the further advancement of brain MRE towards clinical examinations, standardized protocols of wave excitation, image acquisition and image analysis are needed. For wave excitation, the proposed driver offers an easy-to-implement alternative to drivers which have to be adapted to vendor-specific MRI hardware, such as radiofrequency coils or patient tables.

As the focus of our study was the introduction of 'patient and operator friendly' vibration generation for cerebral MRE, the parameter maps and viscoelasticity data represent a starting point for in-detail cartography of human brain mechanics. Independent of whether brain MRE is applied to healthy volunteers or patients, a readily accepted (by subjects) method of introducing mechanical vibrations into the cranial cavity is beneficial. The set-up proposed in this study may contribute to future developments of cerebral MRE, as well as to clinical applications of this promising new imaging modality.

In summary, MRE of the brain based on remote excitation of intracranial shear waves was introduced, which eliminates onerous and uncomfortable mechanical stimulations of the head usually required for cerebral MRE. Furthermore, high-resolution maps of the magnitude and phase angle of the complex shear modulus of the midbrain and central cerebrum were presented and complement previous work to develop an atlas of brain mechanical properties. The proposed set-up is likely to enhance and foster the application of cerebral MRE in the clinic by improving patient comfort and acceptance, whilst maintaining the acquisition of high-quality displacement data and concomitant mechanical property images.

Acknowledgement

A.F. gratefully acknowledges the Hanns-Seidel-Foundation for a scholarship funded by the Federal Ministry of Education and Research.

REFERENCES

1. Kruse SA, Rose GH, Glaser KJ, Manduca A, Felmlee JP, Jack CR, Jr, Ehman RL. Magnetic resonance elastography of the brain. NeuroImage 2008; 39(1): 231–237.

2. Green MA, Bilston LE, Sinkus R. In vivo brain viscoelastic properties measured by magnetic resonance elastography. NMR Biomed. 2008; 21(7): 755–764.
3. Sack I, Beierbach B, Hamhaber U, Klatt D, Braun J. Non-invasive measurement of brain viscoelasticity using magnetic resonance elastography. NMR Biomed 2008; 21(3): 265–271.
4. Wuerfel J, Paul F, Beierbach B, Hamhaber U, Klatt D, Papazoglou S, Zipp F, Martus P, Braun J, Sack I. MR-elastography reveals degradation of tissue integrity in multiple sclerosis. NeuroImage 2010; 49(3): 2520–2525.
5. Streitberger KJ, Sack I, Krefting D, Pfuller C, Braun J, Paul F, Wuerfel J. Brain viscoelasticity alteration in chronic-progressive multiple sclerosis. PLoS One 2012; 7(1e29888).
6. Murphy MC, Huston J, 3rd, Jack CR, Jr, Glaser KJ, Manduca A, Felmlee JP, Ehman RL. Decreased brain stiffness in Alzheimer's disease determined by magnetic resonance elastography. J. Magn. Reson. Imaging 2011; 34(3): 494–498.
7. Lipp A, Trbojevic R, Paul F, Fehlner A, Hirsch S, Scheel M, Noack C, Braun J, Sack I. Cerebral magnetic resonance elastography in supranuclear palsy and idiopathic Parkinson's disease. NeuroImage Clin. 2013; 3: 381–387.
8. Romano A, Scheel M, Hirsch S, Braun J, Sack I. In vivo waveguide elastography of white matter tracts in the human brain. Magn. Reson. Med. 2012; 68(5): 1410–1422.
9. Streitberger KJ, Wiener E, Hoffmann J, Freimann FB, Klatt D, Braun J, Lin K, McLaughlin J, Sprung C, Klingebiel R, Sack I. In vivo viscoelastic properties of the brain in normal pressure hydrocephalus. NMR Biomed. 2011; 24(4): 385–392.
10. Freimann FB, Streitberger KJ, Klatt D, Lin K, McLaughlin J, Braun J, Sprung C, Sack I. Alteration of brain viscoelasticity after shunt treatment in normal pressure hydrocephalus. Neuroradiology 2012; 54(3): 189–196.
11. Murphy MC, Huston J, 3rd, Glaser KJ, Manduca A, Meyer FB, Lanzino G, Morris JM, Felmlee JP, Ehman RL. Preoperative assessment of meningioma stiffness using magnetic resonance elastography. J. Neurosurg 2013; 118(3): 643–648.
12. Simon M, Guo J, Papazoglou S, Scholand-Engler H, Erdmann C, Melchert U, Bonsanto M, Braun J, Petersen D, Sack I, Wuerfel J. Non-invasive characterization of intracranial tumors by MR-Elastography. New J. Phys. 2013; 15: 085024.
13. Schregel K, Wuerfel E, Garteiser P, Gemeinhardt I, Prozorovski T, Aktas O, Merz H, Petersen D, Wuerfel J, Sinkus R. Demyelination reduces brain parenchymal stiffness quantified in vivo by magnetic resonance elastography. Proc. Natl. Acad. Sci. USA 2012; 109(17): 6650–6655.
14. Murphy MC, Curran GL, Glaser KJ, Rossman PJ, Huston J, 3rd, Poduslo JF, Jack CR, Jr, Felmlee JP, Ehman RL. Magnetic resonance elastography of the brain in a mouse model of Alzheimer's disease: initial results. Magn. Reson. Imaging 2011; 30(4): 535–539.
15. Riek K, Millward JM, Hamann I, Mueller S, Pfueller CF, Paul F, Braun J, Infante-Duarte C, Sack I. Magnetic resonance elastography reveals altered brain viscoelasticity in experimental autoimmune encephalomyelitis. NeuroImage Clin 2012; 1(1): 81–90.
16. Freimann FB, Muller S, Streitberger KJ, Guo J, Rot S, Ghori A, Vajkoczy P, Reiter R, Sack I, Braun J. MR elastography in a murine stroke model reveals correlation of macroscopic viscoelastic properties of the brain with neuronal density. NMR Biomed. 2013; 26(11): 1534–1539.
17. Johnson CL, McGarry MD, Gharibans AA, Weaver JB, Paulsen KD, Wang H, Olivero WC, Sutton BP, Georgiadis JG. Local mechanical properties of white matter structures in the human brain. NeuroImage 2013; 79: 145–152.
18. Guo J, Hirsch S, Fehlner A, Papazoglou S, Scheel M, Braun J, Sack I. Towards an elastographic atlas of brain anatomy. PLoS One 2013; 8 (8e71807).
19. Murphy MC, Huston J, 3rd, Jack CR, Jr, Glaser K, Senjem ML, Chen J, Manduca A, Felmlee J, Ehman RL. Measuring the characteristic topography of brain stiffness with magnetic resonance elastography. PLoS One 2013; 8(12e81668).
20. Weaver JB, Pattison AJ, McGarry MD, Perreard IM, Swienckowski JG, Eskey CJ, Lollis SS, Paulsen KD. Brain mechanical property measurement using MRE with intrinsic activation. Phys. Med. Biol. 2012; 57 (22): 7275–7287.
21. Hamhaber U, Klatt D, Papazoglou S, Hollmann M, Stadler J, Sack I, Bernarding J, Braun J. In vivo magnetic resonance elastography of human brain at 7 T and 1.5 T. J. Magn. Reson. Imaging 2010; 32(3): 577–583.
22. Murphy MC, Glaser KJ, Manduca A, Felmlee JP, Huston J 3rd, Ehman RL. Analysis of time reduction methods for magnetic resonance elastography of the brain. Magn. Reson. Imaging, 2010; 28(10): 1514–1524.
23. Clayton EH, Genin GM, Bayly PV. Transmission, attenuation and reflection of shear waves in the human brain. J. R. Soc. Interface 2012; 9(76): 2899–2910.
24. Latta P, Gruwel ML, Debergue P, Matwiy B, Sboto-Frankenstein UN, Tomanek B. Convertible pneumatic actuator for magnetic resonance elastography of the brain. Magn. Reson. Imaging 2011; 29(1): 147–152.
25. Johnson CL, McGarry MD, Van Houten EE, Weaver JB, Paulsen KD, Sutton BP, Georgiadis JG. Magnetic resonance elastography of the brain using multishot spiral readouts with self-navigated motion correction. Magn. Reson. Med. 2013; 70(2): 404–412.
26. Gallichan D, Robson MD, Bartsch A, Miller KL. TREMR: Table-resonance elastography with MR. Magn. Reson. Med. 2009; 62(3): 815–821.
27. Manduca A, Oliphant TE, Dresner MA, Mahowald JL, Kruse SA, Amromin E, Felmlee JP, Greenleaf JF, Ehman RL. Magnetic resonance elastography: non-invasive mapping of tissue elasticity. Med. Image Anal. 2001; 5(4): 237–254.
28. Doyley MM. Model-based elastography: a survey of approaches to the inverse elasticity problem. Phys. Med. Biol. 2012; 57(3): R35–R73.
29. Papazoglou S, Hirsch S, Braun J, Sack I. Multifrequency inversion in magnetic resonance elastography. Phys. Med. Biol. 2012; 57(8): 2329–2346.
30. Hirsch S, Klatt D, Freimann F, Scheel M, Braun J, Sack I. In vivo measurement of volumetric strain in the human brain induced by arterial pulsation and harmonic waves. Magn. Reson. Med. 2012; 70(3): 671–683.
31. Rump J, Klatt D, Braun J, Warmuth C, Sack I. Fractional encoding of harmonic motions in MR elastography. Magn. Reson. Med. 2007; 57(2): 388–395.
32. Streitberger K-J, Reiss-Zimmermann M, Freimann FB, Bayerl S, Guo J, Arlt F, Wuerfel J, Braun J, Hoffmann KT, Sack I. High-resolution mechanical imaging of glioblastoma by multifrequency magnetic resonance elastography. PLoS One 2014; 9(10e110588).
33. McGarry MDJ, Van Houten EEW, Perrinez PR, Pattison AJ, Weaver JB, Paulsen KD. An octahedral shear strain-based measure of SNR for 3D MR elastography. Phys. Med. Biol. 2011; 56(13): N153–N164.
34. Sack I, Joehrens K, Wuerfel E, Braun J. Structure sensitive elastography: on the viscoelastic powerlaw behavior of in vivo human tissue in health and disease. Soft Matter 2013; 9(24): 5672–5680.
35. Yin M, Talwalkar JA, Glaser KJ, Manduca A, Grimm RC, Rossman PJ, Fidler JL, Ehman RL. Assessment of hepatic fibrosis with magnetic resonance elastography. Clin. Gastroenterol. Hepatol. 2007; 5(10): 1207–1213 e1202.
36. Klatt D, Johnson CL, Magin RL. Simultaneous, multidirectional acquisition of displacement fields in magnetic resonance elastography of the in vivo human brain. J. Magn. Reson. Imaging. 2015; 42(3): 297–304.
37. McGarry MDJ, Johnson CL, Sutton BP, Georgiadis JG, Van Houten EE, Pattison AJ, Weaver JB, Paulsen KD. Suitability of poroelastic and viscoelastic mechanical models for high and low frequency MR elastography. Med. Phys. 2015; 42(2): 947–957.
38. Johnson CL, Holtrop JL, McGarry MD, Weaver JB, Paulsen KD, Georgiadis JG, Sutton BP. 3D multislab, multishot acquisition for fast, whole-brain MR elastography with high signal-to-noise efficiency. Magn. Reson. Med. 2014; 71(2): 477–485
39. Braun J, Guo J, Lützkendorf R, Stadler J, Papazoglou S, Hirsch S, Sack I, Bernarding J. High-resolution mechanical imaging of the human brain by three-dimensional multifrequency magnetic resonance elastography at 7T. NeuroImage, 2014; 90: 308–314.
40. Zhang J, Green MA, Sinkus R, Bilston LE. Viscoelastic properties of human cerebellum using magnetic resonance elastography. J. Biomech. 2011; 44(10): 1909–1913.
41. Arani A, Murphy MC, Glaser KJ, Manduca A, Lake DS, Kruse SA, Jack CR Jr, Ehman RL, Huston J 3rd. Measuring the effects of aging and sex on regional brain stiffness with MR elastography in healthy older adults. NeuroImage, 2015; 111: 59–64.
42. Reiss-Zimmermann M, Streitberger KJ, Sack I, Braun J, Arlt F, Fritzsch D, Hoffmann KT. High resolution imaging of viscoelastic properties of intracranial tumours by multi-frequency magnetic resonance elastography. Clin. Neuroradiol. 2014. doi: 10.1007/s00062-014-0311-9.